RSC Advances

PAPER

View Article Online
View Journal | View Issue

Cite this: *RSC Adv.*, 2023, **13**, 32028

Preparation of electrochemical horseradish peroxidase biosensor with black phosphorene–zinc oxide nanocomposite and their applications

Feng Yang,†[ab] Yijing Ai,†[a] Xiaoqing Li,*[c] Lisi Wang,[a] Zejun Zhang,[a] Weipin Ding*[b] and Wei Sun *[a]

Received 30th July 2023
Accepted 17th October 2023

DOI: 10.1039/d3ra05148j

rsc.li/rsc-advances

In this work, a novel and sensitive electrochemical biosensor was constructed based on a black phosphorene (BP) and nanosized zinc oxide (ZnO@BP) nanocomposite as a modifier, which was used for the immobilization of horseradish peroxidase (HRP) on a carbon ionic liquid electrode (CILE). The ZnO@BP nanocomposite was synthesized by a simple *in situ* hydrothermal method with stripped black phosphorus nanoplates and ZnO. The ZnO@BP and HRP-modified electrode was developed by a casting method. ZnO@BP with highly conductivity, large surface area and good biocompatibility could maintain the bioactivity of HRP and accelerate the electron transfer rate. Cyclic voltammetry was used to study the direct electrochemistry of HRP on the Nafion/HRP/ZnO@BP/CILE with the appearance of a pair of distinct redox peaks. The constructed electrochemical HRP biosensor exhibited excellent electrocatalytic effects on the reduction of trichloroacetic acid and sodium nitrite. Real samples were detected with satisfactory results, which demonstrated the potential applications of this electrochemical HRP biosensor.

1. Introduction

Two-dimensional nanomaterials have attracted extensive attention and research interest due to the large specific surface area, unique surface energy and high interfacial reaction activity, which demonstrate a wide range of applications in supercapacitance, photocatalysis, and biosensing.[1–3] In the field of electrochemical biosensors, the electrode interface modified with two-dimensional nanomaterials not only exhibits high affinity and good biocompatibility for biomolecules, but also maintains the activity of biomolecules. Furthermore, the excellent electrical conductivity can significantly enhance the current signal and improve the detection sensitivity.[4] In 2014, single-layer and few-layer black phosphorene (BP) nanosheets were first mechanically stripped from bulk black phosphorus crystals.[5] The synthesis of BP, a new member of the two-dimensional material family, and BP-related composites with high chemical activity, excellent carrier mobility, and anisotropic electrical and thermal conductivities has become a new trend, which act as promising materials for sensing applications.[6–8] For example, Niu *et al.* used a BP-modified glassy carbon electrode (GCE) for the sensitive voltammetric detection of rutin.[9] Li *et al.* prepared an electrochemical biosensor based on BP and a poly(3,4-ethylenedioxythiophene)–poly(styrenesulfonate) composite with hemoglobin (Hb).[10] Zhao *et al.* developed an Hb-biosensor based on poly-L-lysine and BP to investigate the bioactivity of Hb.[11] Shi *et al.* synthesized nitrogen-doped carbonized polymer dots anchoring few-layer BP and constructed an electrochemical DNA sensor for the determination of *Escherichia coli* O157: H7.[12] Xiang *et al.* designed a novel electrochemical nanosensor based on BP for the sensitive voltammetric detection of ochratoxin A in beer and grape juice samples.[13] Ge *et al.* used BP, Nafion and isopropanol composite-modified GCEs for the voltammetric detection of clenbuterol in bovine meat and bovine serum samples.[14] Ramalingam *et al.* constructed a microfluidic aptasensor based on BP and gold nanocomposite-modified screen printed electrodes for the detection of okadaic acid.[15]

As a commonly semiconductive nanomaterial, nano-zinc oxide (ZnO) has been widely selected for the preparation of electrochemical sensors due to its good biocompatibility, high surface activity and low cost.[16,17] Ding *et al.* used a black phosphorous quantum dot (BPQD)-doped ZnO nanoparticle-modified GCE for the detection of hydrogen peroxide with excellent electrochemical properties.[18] Li *et al.* synthesized a BP–ZnO nanohybrid by a simple one-step co-precipitation method with enhanced visible light photocatalytic activity.[19] Li *et al.* constructed a NO_2 sensing platform based on hetero-structured ZnO–BP composites to detect NO_2 gas.[20]

[a]*Key Laboratory of Laser Technology and Optoelectronic Functional Materials of Hainan Province, Key Laboratory of Functional Materials and Photoelectrochemistry of Haikou, College of Chemistry and Chemical Engineering, Hainan Normal University, Haikou 571158, China. E-mail: sunwei@hainnu.edu.cn*

[b]*Haikou Marine Geological Survey Center, China Geological Survey, Haikou, 571127, China. E-mail: gzsdingwp@126.com*

[c]*College of Health Sciences, Shandong University of Traditional Chinese Medicine, Jinan, 250355, China. E-mail: l1x2q3_li@126.com*

† These authors contributed equally to this work.

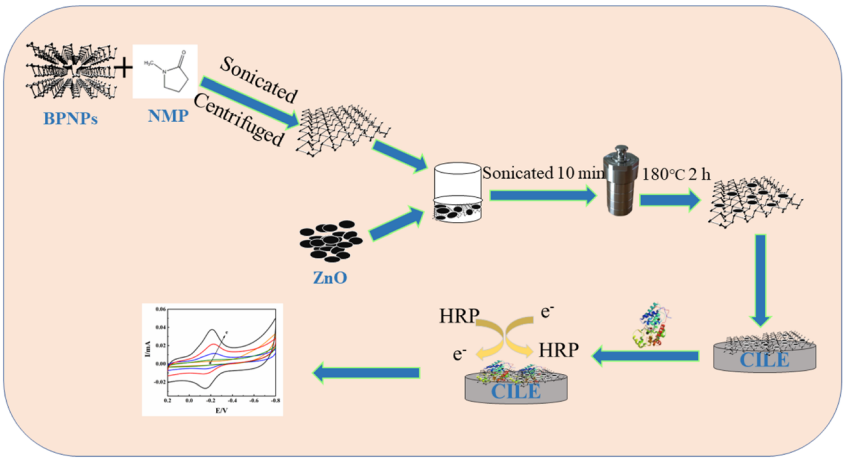

Scheme 1 Experimental process diagram for the synthesis of ZnO@BP nanocomposite and the fabrication procedure of electrochemical biosensor.

In this paper, ZnO@BP was synthesized by an *in situ* hydrothermal method and modified on the surface of a carbon ionic liquid electrode (CILE) as a substrate electrode. Horseradish peroxidase (HRP) was immobilized on the ZnO@BP/CILE with Nafion as a film to obtain the biosensor. The synthesis of a ZnO@BP nanocomposite and the fabrication procedure of the electrochemical biosensor are shown in Scheme 1. Due to the synergistic properties between BP and ZnO, direct electrochemical behaviors of HRP on the modified electrode exhibited a pair of quasi-reversible redox peaks. Furthermore, the modified electrode was used for the electrocatalytic reduction of trichloroacetic acid (TCA) and sodium nitrite ($NaNO_2$) with satisfactory results.

2. Experimental

2.1 Reagents

1-Hexylpyridinium hexafluorophosphate ($HPPF_6$, >99%, Lanzhou Yulu Fine Chem. Co., Ltd., China), HRP (MW 40 000, Sinopharm Chem. Reagent Co., Ltd., China), black phosphorus nanoplate dispersion (BPNPs, Nanjing XFNANO Materials Tech. Co., Ltd., China), 1-methyl-2-pyrrolidone (NMP, 99.5%, Shanghai Aladdin Bio-Chem. Tech. Co., Ltd., China), TCA (Tianjin Kemiou Chem. Co., Ltd., China), nano-zinc oxide (ZnO, Nanjing XFNANO Materials Tech. Co., Ltd., China), $NaNO_2$ (Yantai Sahe Chem, Co., Ltd., China) and graphite powder (particle size 30 μm, Shanghai Colloid Chem. Co., Ltd., China) were used as provided. The supporting electrolyte was 0.1 mol per L phosphate buffer solution (PBS) with different pH values. All the other reagents were of analytical grade, and ultra-pure water (Milli-Q, IQ-7000, Merck Millipore Co., Ltd., USA) was used throughout the experiments.

2.2 Apparatus

All the electrochemical experiments were performed using a CHI 1040C electrochemical workstation (Shanghai Chenhua Instrument Co., Ltd., China). Electrochemical impedance spectroscopy (EIS) was carried out using a CHI 660E electrochemical workstation (Shanghai Chenhua Instrument Co., Ltd., China). A traditional three-electrode system was used with a self-made modified electrode (Nafion/HRP/ZnO@BP/CILE) as the working electrode, Ag/AgCl (saturated KCl solution) as the reference electrode, and a platinum wire as the auxiliary electrode. Transmission electron microscopy (TEM) was performed using a JEM-2010F (JEOL, Japan) with scanning electron microscopy (SEM) using a JSM-7100F (JEOL, Japan). X-ray diffraction (XRD) experiments were conducted using a D/Max-2500V X-ray diffractometer (Rigaku, Japan) with Cu-Kα radiation. X-ray photoelectron spectroscopy (XPS) was performed using an AXIS HIS 165 spectrometer (Kratos Analytical, UK). The N_2 adsorption and desorption isotherms, surface area and pore size distribution of the ZnO@BP nanocomposite were tested using an Autosorb iQ Station 2 (Quantachrome Instruments, USA) in a liquid nitrogen environment.

2.3 Synthesis of ZnO@BP nanocomposite

According to the reported procedure with slight modifications,[21,22] 10.0 mg BPNP powder and 10.0 mL of NMP were mixed in a mortar and then ground for 10 min. The mixture was sonicated for 8 h with ice cooling and then centrifuged at 8000 rpm for 20 min to remove unexfoliated BPNPs and obtain a BP suspension. ZnO@BP was synthesized by an *in situ* hydrothermal method as follows:[23] first, 10.0 mL 1.0 mg mL^{-1} nano-ZnO dispersion was added into 10.0 mL as-obtained BP suspension. The mixture solution was sonicated for 10 min and sealed into a Teflon equipped stainless steel autoclave. After heating at 180 °C for 2 h, the product was removed, washed with ethanol solution and N_2 saturated ultrapure water, respectively, and dried at 60 °C for 8 h under vacuum to obtain a ZnO@BP solid powder.

2.4 Construction of the modified electrode

According to the ref. 24, the mass ratio of graphite powder and $HPPF_6$ was 2 : 1 to construct a CILE, which was used as the

base electrode with the electrode surface polished before each use. In a nitrogen-filled glove box, 10.0 μL of 1.0 mg mL^{-1} ZnO@BP suspension was casted onto the surface of the electrode and dried naturally to obtain the ZnO@BP/CILE. Then, 10.0 μL of 15.0 mg mL^{-1} HRP solution and 10.0 μL of 0.5% Nafion solution were applied onto the modified surface in sequence and dried at room temperature to obtain the Nafion/HRP/ZnO@BP/CILE. The same method and procedure were used to fabricate other modified electrodes for comparison.

2.5 Electrochemical investigations

Electrochemical measurements were investigated in 0.1 mol L^{-1} PBS with different pH values ranging from 2.0 to 8.0 by cyclic voltammetry (CV) at a scan rate of 0.1 V s^{-1}. The buffer solutions were deoxygenated by highly pure nitrogen for 20 min before the measurements. Electrochemical behaviors of different modified electrodes were analyzed in 1.0 mmol L^{-1} $K_3[Fe(CN)_6]$ and 0.5 mol L^{-1} KCl solution with EIS measurements in 10.0 mmol L^{-1} $K_3[Fe(CN)_6]/K_4[Fe(CN)_6]$ and 0.1 mol L^{-1} KCl solution in the frequency range of 0.1–10^5 Hz.

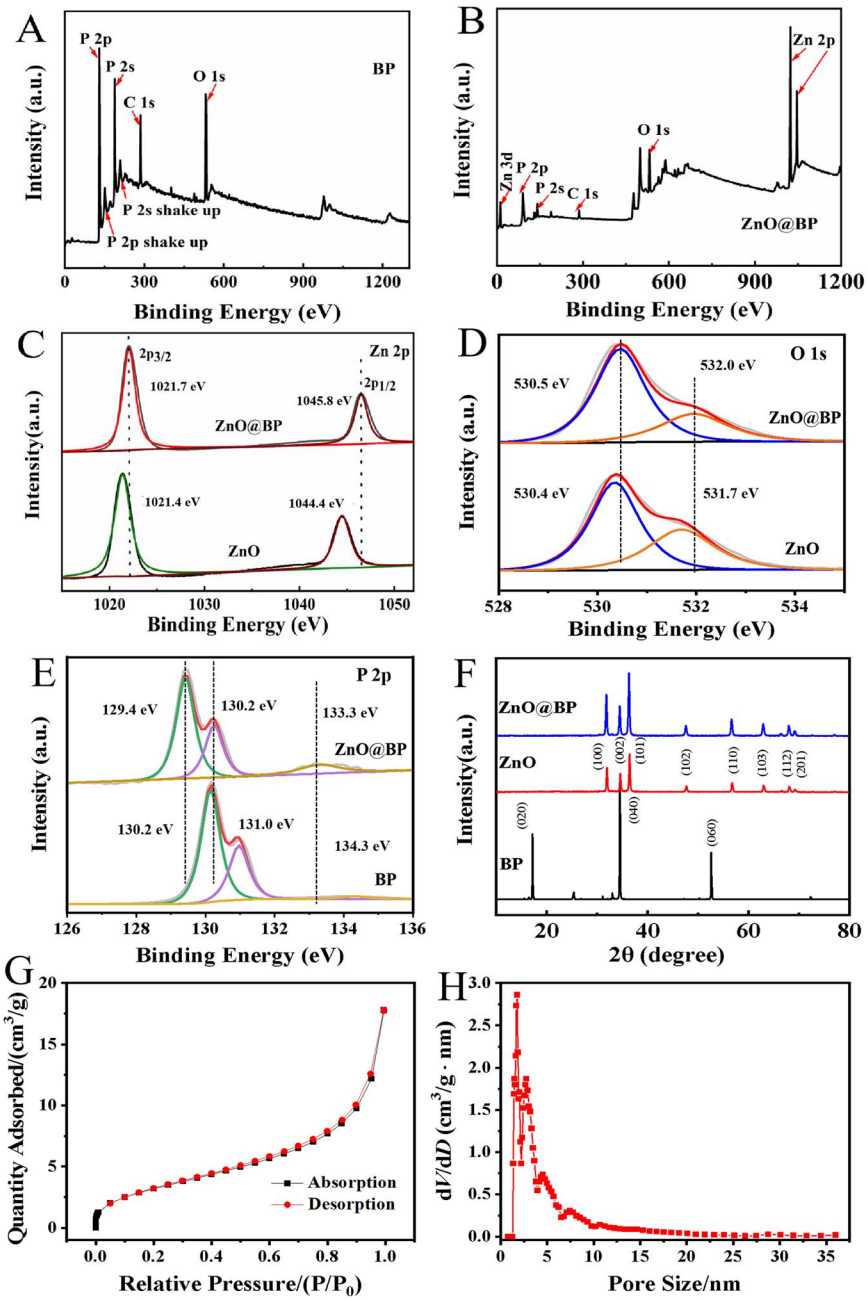

Fig. 1 Survey XPS spectra of (A) BP and (B) ZnO@BP nanocomposites. (C) Zn 2p, (D) O 1s and (E) P 2p spectra of ZnO and ZnO@BP nanocomposites. (F) XRD patterns of BP, ZnO and ZnO@BP nanocomposites. (G) N_2 adsorption and desorption isotherms of ZnO@BP nanocomposites. (H) Pore size distribution curve.

3. Results and discussion

3.1 Characterization of ZnO@BP nanocomposite

XPS was performed to illustrate the composition and chemical state of elements in materials. In Fig. 1A and B, the full survey spectra of BP and ZnO@BP confirmed the presence of O, P and Zn, in which the atom ratio of Zn 2p and P 2p was 19 : 25. Fig. 1C showed the characteristic peaks of pure ZnO at 1021.4 eV and 1044.4 eV, which were ascribed to the binding energies of Zn $2p_{3/2}$ and Zn $2p_{1/2}$, respectively.[25] Compared with pure ZnO, the characteristic peaks of Zn $2p_{3/2}$ and Zn $2p_{1/2}$ for ZnO@BP shifted 0.3 eV and 1.4 eV to a higher binding energy, respectively. Fig. 1D shows the O 1s XPS spectra of ZnO and ZnO@BP, and the peaks at 530.4 eV and 530.5 eV were assigned to the O^{2-} ions in the Zn–O bonding of ZnO and ZnO@BP.[26] Besides, the shoulder peaks at 531.7 eV and 532.0 eV were related to surface-adsorbed oxygen of materials, which also moved to higher binding energies. For XPS P 2p spectra (Fig. 1E), three characteristic peaks located at 130.2 eV, 131.0 eV and 134.3 eV for BP were attributed to P $2p_{3/2}$, P $2p_{1/2}$ and oxidized phosphorus (PO_x).[27] The characteristic peaks of P $2p_{3/2}$ and P $2p_{1/2}$ for ZnO@BP both shifted to lower binding energies (129.4 eV and 130.2 eV, respectively), which indicated the electron transfer from ZnO to BP and strong interaction between ZnO and BP nanosheets. Besides, the peak intensity of PO_x increased and the binding energy changed 1.0 eV, indicating the slight oxidation of BP nanosheets during the preparation of ZnO@BP.

Fig. 1F further shows the XRD pattern of nano-ZnO, BP and ZnO@BP nanocomposites. As for pure nano-ZnO particles, XRD analysis showed that the reflections at 2θ were 31.89°, 34.57°, 36.48°, 47.70°, 56.89°, 63.03°, 68.11°, and 69.17°, which corresponded to the (100), (002), (101), (102), (110), (103), (112) and (201) crystal planes of single-phase ZnO with the wurtzite structure (JCPDS file no. 36-1451).[28,29] For BP, three strong peaks at 16.92°, 34.22° and 52.34° were assigned to the (020), (040) and (060) planes of BP (JCPDS file no. 47-1626), respectively. The weak peaks of BP in Fig. 1F might correspond to a slightly distorted orthorhombic structure of BP.[30] Due to the low doping amount of BP, the typical diffraction peak of BP could not be detected in ZnO@BP. The lattice parameters of ZnO@BP were very similar to those of pure ZnO, indicating that the influence of BP lattice on the lattice parameters of ZnO was negligible. It was inferred that ZnO was only dispersed on the surface of BP and maintained good crystal lattice.[19]

The textural properties of ZnO@BP were further studied by the N_2 adsorption–desorption analyses. As shown in Fig. 1G, the adsorption–desorption isotherm profile was described as type IV, which indicated that ZnO@BP has abundant mesoporous and macroporous structures with a BET specific surface area of 11.7 $m^2\ g^{-1}$. The pore distribution plot is depicted in Fig. 1H, and ZnO@BP exhibits a pore size distribution from 1.3 to 3.5 nm with a peak at 1.76 nm. The presence of mesoporous and macroporous structures of ZnO@BP was ascribed to the immobilization of HRP.

Fig. 2 shows the SEM and TEM images of BPNPs, ZnO and ZnO@BP nanocomposites. It could be observed that the BPNPs presented a multilayered sheet-like structure (Fig. 2A and B) and ZnO appeared as nanoparticles with some aggregations (Fig. 2C and D). Fig. 2E and F show the typical SEM images of ZnO@BP nanocomposites at different amplifications, which indicated that the existence of BP reduced the stacking density of ZnO nanoparticles. The TEM image (Fig. 2G) indicated that ZnO nanoparticles were successfully loaded on the BP nanosheets. The elemental mapping images of P, Zn and O (Fig. 2H) indicated that all the elements were uniformly distributed on the surface of ZnO@BP.

3.2 Electrochemical characterizations

Using 1.0 mmol L^{-1} $K_3[Fe(CN)_6]$ and 0.5 mol L^{-1} KCl mixture as the electrochemical probe, electrochemical responses of different modified electrodes were investigated by CV. As shown in Fig. 3, on the CILE (curve a) a pair of reversible redox peak appeared with a cathodic peak current (I_{pc}) of 19.80 μA and an

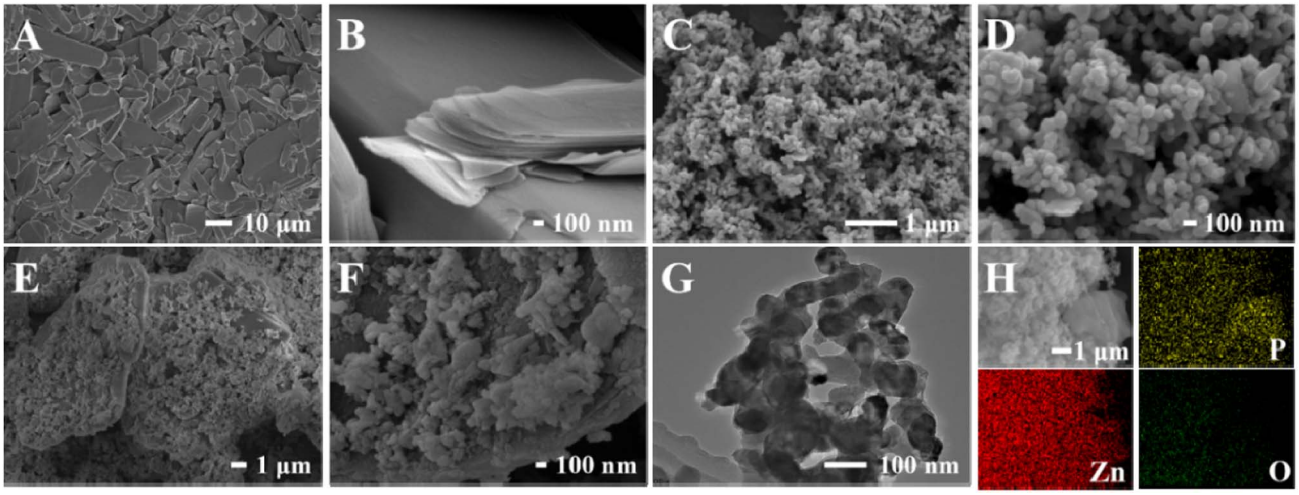

Fig. 2 SEM images of (A and B) BPNPs, (C and D) ZnO, and (E and F) ZnO@BP nanocomposites with different magnification. (G) TEM image of ZnO@BP nanocomposites. (H) Elemental mapping of P, Zn and O of ZnO@BP nanocomposites.

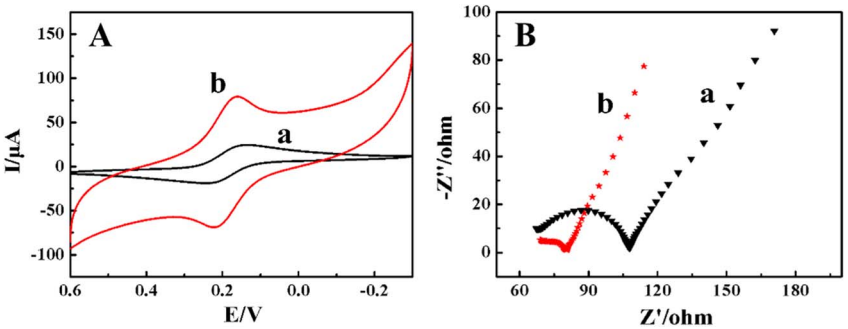

Fig. 3 (A) Cyclic voltammograms of the CILE (curve a) and ZnO@BP/CILE (curve b) in 1.0 mmol L^{-1} $K_3[Fe(CN)_6]$ and 0.5 mol L^{-1} KCl solution at a scan rate of 100 mV s^{-1} (B) EIS results of the CILE (curve a) and ZnO@BP/CILE (curve b) in 10.0 mmol L^{-1} $K_3[Fe(CN)_6]/K_4[Fe(CN)_6]$ and 0.1 mol L^{-1} KCl solution at a frequency from 10^5 to 0.1 Hz.

anodic peak current (I_{pa}) of 17.80 μA. The anodic peak potential (E_{pa}) and cathodic peak potential (E_{pc}) were located at 0.249 V and 0.164 V with the peak-to-peak separation (ΔE_p) of 85 mV. As for the ZnO@BP/CILE (curve b), the I_{pc} and I_{pa} were increased to 48.12 μA and 43.16 μA, respectively, which were 2.43 and 2.42 times than that of the bare CILE with a ΔE_p value decreased to 65 mV, which indicated that the redox reaction of $[Fe(CN)_6]^{3-/4-}$ became more reversible.[31] Therefore, the modification of ZnO@BP on the CILE surface significantly improved the interfacial conductivity of the modified electrode, accelerated the electron transfer rate of $[Fe(CN)_6]^{3-/4-}$, and improved the electrochemical response signal.

EIS is commonly used to investigate the electron–hole separation efficiency.[32] The electron transfer resistance (R_{et}) depends on the semicircle domains of impedance spectra and can control the electron-transfer kinetics of the redox probe on the electrode surface. As shown in Fig. 3B, on the bare CILE (curve a) R_{et} was estimated to be 22 Ω, which was due to the high conductivity of the CILE. As for the ZnO@BP/CILE (curve b), the R_{et} was approximately 10 Ω, which was lower than that of the bare CILE, indicating that the ZnO@BP nanocomposite present on the surface of CILE provided a faster electron transfer process at the interface due to the high conductivity. The corresponding electrochemical parameters are listed in Table 1 for comparison. Based on the Randles–Sevcik equation,[33,34] the effective electrode surface area of the ZnO@BP/CILE was calculated as 0.207 cm^2, which was 1.64 times larger than that of the CILE (0.126 cm^2). Therefore, the presence of ZnO@BP nanocomposite can not only provide a large effective surface area, but also improve the interfacial conductivity. The synergistic effects resulted in an increase in the current response of electrochemical probes with a more reversible electrode process.

Table 1 Electrochemical parameters of different electrodes

Electrodes	I_{pc} (μA)	I_{pa} (μA)	E_{pc} (mV)	E_{pa} (mV)	ΔE (mV)	R_{et} (Ω)
CILE	19.80	17.80	0.164	0.249	85	22
ZnO@BP/CILE	48.12	43.16	0.159	0.224	65	10

3.3 Direct electrochemistry

In 0.1 mol L^{-1} pH 2.0 PBS, the electrochemical behaviors of different modified electrodes were investigated by CV with curves shown in Fig. 4A, no voltammetric responses were observed on the bare CILE (curve a) and Nafion/ZnO@BP/CILE (curve b), indicating that no electrochemical reaction took place on the electrodes in the potential range of −0.8 to 0.2 V. On the Nafion/HRP/CILE (curve c), a pair of redox peaks appeared with I_{pc} as 5.456 μA and I_{pa} as 3.521 μA, indicating that the electron transfer of HRP had occurred on the electrode surface. E_{pa} and E_{pc} were located at −0.234 V and −0.142 V with ΔE_p as 92 mV and I_{pa}/I_{pc} as 0.65, demonstrating a quasi-reversible electrode process.[35] On the Nafion/HRP/ZnO/CILE (curve d), a larger redox peak current appeared with the I_{pc} and I_{pa} increased to 16.07 μA and 11.03 μA, respectively, indicating that the presence of ZnO could improve the response. While on the Nafion/HRP/ZnO@BP/CILE (curve e), a more reversible redox peak appeared with the largest redox currents and a well-defined peak shape. The current value of I_{pc} (22.40 μA) and I_{pa} (16.85 μA) were 4.11 and 4.79 times than those of the Nafion/HRP/CILE, respectively, revealing that ZnO@BP could promote the electron transfer of HRP effectively. It was attributed to the synergistic effects of the ZnO@BP nanocomposite with a larger effective surface area, high conductivity, increased interfacial roughness, more exposed active sites and good biocompatibility, which promoted the direct electron transfer rate and improved the electrochemical response signal. E_{pc} and E_{pa} were located at −0.210 V and −0.148 V with ΔE as 62 mV and the formal peak potential $[E^{0\prime} = (E_{pa} + E_{pc})/2]$ as −0.179 V, which was characteristic of HRP Fe(III)/Fe(II) redox couples.[36] The results indicated that the HRP molecules maintained the active structure in the composite film with direct electron transfer of HRP accelerated by the ZnO@BP nanocomposite on the substrate electrode.

The influence of scan rate in the range of 0.05 to 1.0 V s^{-1} on the direct electrochemical behavior of HRP was also investigated by CV with the results shown in Fig. 4B. It can be found that the redox peak current gradually increased and the peak potential slightly shifted with the increase in scanning rate. The redox peak potential had a linear relationship with ln ν and the corresponding linear regression equations were calculated as

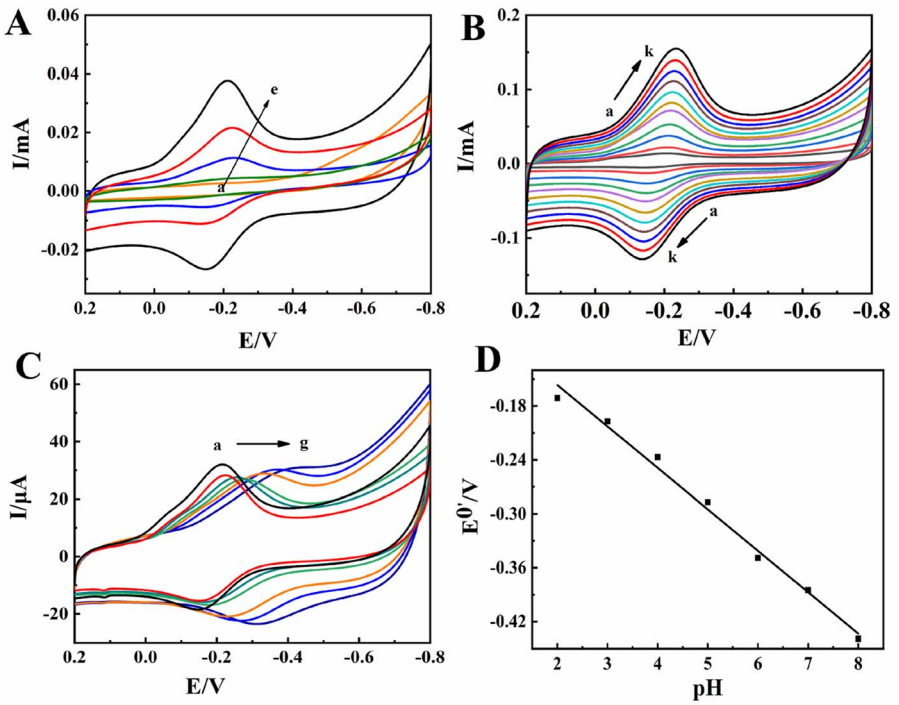

Fig. 4 (A) Cyclic voltammograms of (a) CILE, (b) Nafion/ZnO@BP/CILE, (c) Nafion/HRP/CILE, (d) Nafion/HRP/ZnO/CILE and (e) Nafion/HRP/ZnO@BP/CILE in pH 2.0 PBS at a scan rate of 100 mV s^{-1}. (B) Cyclic voltammograms of the Nafion/HRP/ZnO@BP/CILE at different scan rates in pH 2.0 PBS (from (a)–(k): 0.05, 0.1, 0.2, 0.3, 0.4, 0.5, 0.6, 0.7, 0.8, 0.9, 1.0 V s^{-1}). (C) Cyclic voltammograms of Nafion/HRP/ZnO@BP/CILE in PBS of different pH values ((a)–(g) represent the pH values of 2.0, 3.0, 4.0, 5.0, 6.0, 7.0, and 8.0) at a scan rate of 100 mV s^{-1}. (D) Linear relationship between $E^{0\prime}$ and pH.

E_{pa} (V) = 0.0492 ln ν − 0.1117 (γ = 0.995) and E_{pc} (V) = −0.0525 ln ν − 0.2537 (γ = 0.993). According to Laviron's equation,[37,38] the electron transfer number (n) and the electron transfer coefficient (α) were 0.926 and 0.484. Then, the reaction rate constant (k_s) can be further calculated as 5.93 s^{-1}, which was much larger than previous reports of 1.27 s^{-1},[39] 0.14 s^{-1},[40] and 1.585 s^{-1}.[41] Therefore, the existence of the ZnO@BP nanocomposite can provide a biocompatible interface on the electrode surface, which made HRP undergo a single-electron transfer reaction on the modified electrode with the accelerated electron transfer rate. The redox peak current gradually increased with the scan rate, and there was a linear relationship between the peak currents and scan rate. The linear regression equations were obtained as I_{pc} (μA) = 76.83ν (V s^{-1}) + 3.075 (γ = 0.998) and I_{pa} (μA) = − 63.12ν (V s^{-1}) − 1.761 (γ = 0.998), indicating that the electrochemical reaction at the electrode interface was an adsorption control process. According to the formula $Q = nAF\Gamma^*$,[42] Γ^* was calculated as 5.33 × 10^{-9} mol cm^{-2}, and the total amount of HRP on the modified electrode interface was 2.98 × 10^{-8} mol cm^{-2}. Therefore, 17.9% HRP molecules on the electrode surface participated in the electrode reaction process, which confirmed that the ZnO@BP nanocomposite could make more than one layer of HRP take part in the electrode reaction. Therefore, the ZnO@BP nanocomposite can not only offer a large surface area and high conductivity, but also improve the adsorption and the loading of HRP with the electron transfer rate accelerated. The good electrical conductivity and two-dimensional structure of BP were advantageous to quick charge transfer and ZnO loading, and the effective surface area of ZnO offered more activity sites for HRP binding.

The influence of different pH buffers on the direct electrochemical behavior of HRP in PBS was checked. As shown in Fig. 4C, with the increase in pH from 2.0 to 8.0, the redox peak potential gradually shifted to the negative direction. The formal peak potential ($E^{0\prime}$) has a good linear relationship with pH (Fig. 4D) with the linear regression equation as $E^{0\prime}$ (V) = − 0.0461pH − 0.0643 (γ = 0.991), which showed that the formal peak potential increased by 46.1 mV for each additional pH unit. For the reversible system, the theoretical value of the slope value was 59.0 mV pH^{-1} (298 K) for a single proton-coupled reversible one-electron transfer process.[43,44] The electrochemical reduction process of HRP may be expressed using the equation: HRP Fe(III) + H^+ + e^- ↔ HRP Fe(II).[45] When the pH was 2.0, the cathodic peak current reached the maximum and the electrochemical response signal was the most obvious. This may be attributed to the heme iron and the amino acids around HRP were influenced by the protonation of transligands or the protonation of water molecules coordinated to the heme iron.[46,47] In a pH 2.0 buffer, more hydrogen ions can be provided to traverse the Nafion film and involve in the following electrode reaction. Besides, the Nafion film can protect the sensing interface composed of HRP and ZnO@BP. Therefore, pH 2.0 was selected as the optimal condition for all experiments.

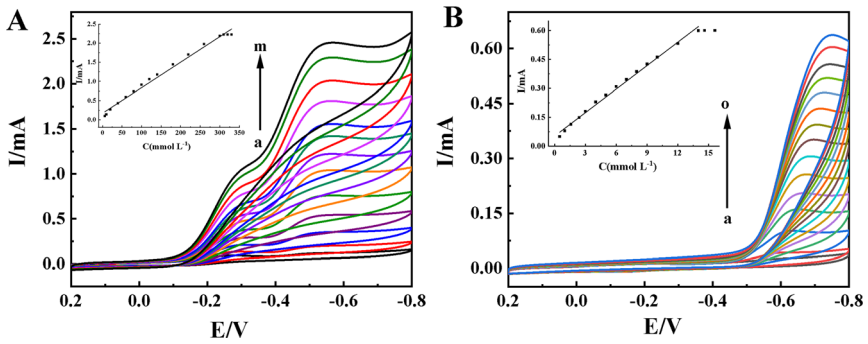

Fig. 5 Cyclic voltammograms of the Nafion/HRP/ZnO@BP/CILE in 0.1 mol L^{-1} pH 2.0 PBS at a scan rate of 100 mV s^{-1} (A) with 0.6, 10.0, 20.0, 40.0, 60.0, 80.0, 100.0, 120.0, 140.0, 180.0, 220.0, 260.0, and 300.0 mmol L^{-1} TCA (curve a–m), the inset shows the relationship of catalytic reduction peak currents and the TCA concentration, and (B) with 0.5, 1.0, 1.6, 2.4, 3.0, 4.0, 5.0, 6.0, 7.0, 8.0, 9.0, 10.0, 12.0, 14.0, and 14.6 mmol L^{-1} $NaNO_2$ (curve a–o), the inset shows the relationship of catalytic reduction peak currents and the $NaNO_2$ concentration.

3.4 Electrocatalytic performance

TCA is widely used in industry, agriculture, biochemistry and public health fields, which is an organohalide environmental pollutant and has been proven to be carcinogenic and poses potential risks to human health.[48,49] Nitrates and nitrites are food preservative and extensively used in the food industry. At a concentration exceeding the safe levels, they pose a wide variety of health risks.[50] Therefore, it is important to develop sensitive electrochemical methods for TCA and $NaNO_2$ detection. It is well known that the redox protein-based electrochemical sensors show excellent electrocatalytic ability toward the reduction of TCA and $NaNO_2$.[51,52]

The electrocatalytic behaviors of the Nafion/HRP/ZnO@BP/CILE to TCA were investigated with CV curves of different concentrations of TCA recorded in Fig. 5A. With the addition of TCA, the reduction peaks current at −0.55 V gradually increased, which was a typical feature of the TCA catalytic reaction. When the TCA concentration was in the range of 0.6 to 300.0 mmol L^{-1}, the reduction peak currents (I_{ss}) had a linear relationship with the TCA concentration, and the linear regression equation was I_{ss} (mA) = 0.0067C (mmol L^{-1}) + 0.168 (γ = 0.991) with the detection limit as 0.2 mmol L^{-1} (3S/N). When the TCA concentration was greater than 300.0 mmol L^{-1}, the reduction peak current remained basically stable, indicating a typical Michaelis–Menten kinetic reaction mechanism. The apparent Michaelis constant (K_M^{app}) can be calculated according to the electrochemical expression of the Lineweaver–Burk equation:[53]

$$\frac{1}{I_{ss}} = \frac{1}{I_{max}} + \frac{K_M^{app}}{I_{max} C}$$

In the formula, I_{ss} is the steady-state current after adding the substrate, C is the concentration of the substrate, and I_{max} is the maximum current measured under the saturated substrate state. Using the double reciprocal plot method ($1/I_p \sim 1/[TCA]$), the apparent Michaelis constant of this catalytic reaction could be calculated as 0.14 mmol L^{-1}, which was smaller than the previous reports, as listed in Table 2. It is well known that the smaller K_M^{app} value showed the higher catalytic ability.[39] Therefore, the HRP-modified electrode based on the ZnO@BP-modified CILE had a high catalytic activity for TCA.

Fig. 5B shows the cyclic voltammograms of the Nafion/HRP/ZnO@BP/CILE in different concentrations of $NaNO_2$ with a reduction peak appearing at −0.62 V (*vs.* SCE). When the concentration of $NaNO_2$ was in the range of 0.5 to 14.6 mmol L^{-1}, I_{ss} had a good linear relationship with the concentration of $NaNO_2$ (inset of Fig. 5B) and the linear regression equation was I_{ss} (mA) = 0.0406C (mmol L^{-1}) + 0.0523 (γ = 0.995) with the detection limit as 0.167 mmol L^{-1} (3S/N). When the

Table 2 Comparison of electrochemical biosensors for the detection of TCA[a]

Modified electrode	Linear range (mmol L^{-1})	Detection limit (mmol L^{-1})	K_M^{app} (mmol L^{-1})	Ref.
AFIL–LDH–Hb/GCE	0.8–430.0	0.19	1.43	39
CTS/Hb/GR–CuS/CILE	1.0–64.0	0.20	6.30	40
CTS/GR–LDH–C_3N_4–Hb/CILE	0.2–36.0	0.05	3.30	45
Hb/ZnO–MWCNTs/Nafion/GCE	1.0–82.6	0.80	—	46
CTS/ELDH–GR–Hb/CILE	5.0–360	1.51	7.90	49
Nafion/Mb–HAp@CNF/CILE	6.0–180.0	2.00	224	54
HA–HRP–CdS–IL/CILE	1.6–18.0	0.53	0.36	55
CTS/TiO_2–Hb/CILE	0.8–32.0	0.26	1.75	56
Nafion/HRP/ZnO@BP/CILE	0.6–300.0	0.20	0.14	This work

[a] AFIL: amino functionalized ionic liquid; LDH: layered double hydroxides; GCE: glassy carbon electrode; GR: graphene, CTS: chitosan; ELDH: exfoliated Co_2Al layered double hydroxide; HAp@CNF: hydroxyapatite doped carbon nanofiber.

Table 3 Comparison of electrochemical biosensors for the detection of $NaNO_2$[a]

Modified electrode	Linear range (mmol L^{-1})	Detection limit (mmol L^{-1})	K_M^{app} (mmol L^{-1})	Ref.
Nafion/Mb–HAp@CNF/CILE	0.3–10.0	0.23	1.13	54
Nafion/Mb/GT/CILE	0.4–4.2	0.13	1.36	57
Nafion/Hb/B-GQDs/CILE	1.0–80.0	0.3	6.37	58
Nafion–Mb–SGO–GCE	2.0–24.5	1.5	—	59
Nafion/Hb/Co_3O_4–CNF/CILE	1.0–12.0	0.33	—	60
Nafion/Mb–SWCNT/GCE	0.5–5.0	0.95	6.45	61
BPE–PEDOT:PSS–hemin/CILE	1.0–10.5	0.33	23.31	62
Nafion/HRP/ZnO@BP/CILE	0.5–14.6	0.17	5.96	This work

[a] GT: graphene tube; B-GQDs: boron-doped graphene quantum dots; SGO: sulfonated graphene oxide; BPE-PEDOT:PSS: black phosphorene (BPE) and poly(3,4-ethylenedioxythiophene)–poly(styrenesulfonate) (PEDOT:PSS) hybrid.

Table 4 Analytical results of TCA and $NaNO_2$ in different samples ($n = 3$)

Sample	Detected (mmol L^{-1})	Added (mmol L^{-1})	Total (mmol L^{-1})	Recovery (%)	RSD
Medical facial peel	10.97	10.00	20.54	95.7	2.71
		20.00	32.58	108.1	3.60
		30.00	42.24	104.2	2.82
Soak water of pickled vegetables	1.12	2.0	3.14	101.0	1.93
		2.5	3.59	98.8	2.11
		3.0	4.13	100.3	1.75

concentration of $NaNO_2$ reached 14.6 mmol L^{-1}, the reduction peak current remained basically unchanged, and then K_M^{app} of the catalytic reaction of the Nafion/HRP/ZnO@BP/CILE can be calculated as 5.96 mmol L^{-1}.

The electrocatalytic activities of the Nafion/HRP/ZnO@BP/CILE and other sensors toward TCA and $NaNO_2$ were compared, and the results are presented in Tables 2 and 3, which indicated the superior activity of the Nafion/HRP/ZnO@BP/CILE to some of the previously reported sensors with a lower detection limit and a wider linear range. All the results concluded that the ZnO@BP nanocomposite provided better biocompatibility and higher enzymatic ability of HRP for TCA and $NaNO_2$ detection, which was attributed to the comprehensive synergy between ZnO and BP.

3.5 Analytical applications

In terms of actual sample application, the modified electrode was used to detect the content of TCA in the medical facing peel solution (Shanghai EKEAR Bio. Tech. Co., Ltd., 35% TCA) and $NaNO_2$ in pickled vegetables (bought from food supermarket and filtered off the mixture) by using the standard addition method. As shown in Table 4, the recovery rates were between 95.7–108.1% and 98.8–101.0% with the relative standard deviation (RSD) less than 4.0%, indicating that the proposed detection method can be used for the analysis of TCA and $NaNO_2$ in actual samples with good application prospects.

3.6 Stability and reproducibility

The stability and reproducibility of the Nafion/HRP/ZnO@BP/CILE were investigated. After scanning continuously for 50 cycles in PBS, the cyclic voltammetric response was reduced by 2.36% as compared with the initial current. The modified electrode was stored in a refrigerator at about 4 °C for two weeks, and the redox peak current remained at 97.2% of the original value. After being placed for four weeks, the cyclic voltammetric response remained at 90.8% of its original value, which proved that the modified electrode had good stability. Three Nafion/HRP/ZnO@BP/CILE were used to detect 10.0 mmol L^{-1} TCA with an RSD value of 3.21%, indicating that the Nafion/HRP/ZnO@BP/CILE had excellent reproducibility for the voltammetric detection of TCA. Therefore, the good stability and excellent reproducibility of the constructed biosensor can be attributed to the high stability of the ZnO@BP nanocomposite on the modified electrode.

4. Conclusion

In this work, a new and sensitive electrochemical biosensor has been prepared based on a ZnO@BP nanocomposite by an *in situ* hydrothermal method, which has been modified on the surface of a CILE. The electrochemical behavior of the Nafion/HRP/ZnO@BP/CILE was investigated by cyclic voltammetry with a pair of quasi-reversible redox peaks observed, indicating that the presence of the ZnO@BP nanocomposite could enhance the electron transfer rate with the advantages of large specific surface area, high electronic conductivity and good biocompatibility. The electrocatalytic behaviors to TCA and $NaNO_2$ were further studied with the characteristics of wider linear range, lower detection limit and good stability. In addition, the proposed electrodes were used to detect the real samples with satisfactory results, which showed that the ZnO@BP

nanocomposite had potential application in the field of electrochemical sensors.

Conflicts of interest

There are no conflicts to declare.

Acknowledgements

This project was financially supported by the China Geological Survey Project "Wetland Resources Survey of International Importance in South China" (DD20220876).

References

1 Y. Y. Shao, J. Wang, H. Wu, J. Liu, I. A. Aksay and Y. H. Liu, Graphene based electrochemical sensors and biosensors: a review, *Electroanalysis*, 2010, **22**, 1027–1036, DOI: **10.1002/elan.200900571**.

2 L. S. Oriol, L. Dominik, K. Metin, R. Aleksandra and K. Andras, Ultrasensitive photodetectors based on monolayer MoS_2, *Nat. Nanotechnol.*, 2013, **8**, 497–501, DOI: **10.1038/nnano.2013.100**.

3 Z. Zhuge, Y. H. Tang, J. W. Tao and Y. Zhao, Functionalized black phosphorus nanocomposite for biosensing, *ChemElectroChem*, 2019, **6**, 1–6, DOI: **10.1002/celc.201801439**.

4 S. Kumar, Y. J. Lei, N. H. Alshareef, M. A. Quevedo-Lopez and K. N. Salama, Biofunctionalized two-dimensional Ti_3C_2 Mxenes for ultrasensitive detection of cancer biomarker, *Biosens. Bioelectron.*, 2018, **121**, 243–249, DOI: **10.1016/j.bios.2018.08.076**.

5 L. K. Li, Y. J. Yu, G. J. Ye, Q. Q. Ge, X. D. Qu, H. Wu, D. L. Feng, X. H. Chen and Y. B. Zhang, Black phosphorus field-effect transistors, *Nat. Nanotechnol.*, 2014, **9**, 372–377, DOI: **10.1038/nnano.2014.35**.

6 J. H. Wu, S. L. Huang, Z. Y. Jin, J. Q. Chen, L. Hu, Y. J. Long, J. G. Lu, S. C. Ruan and Y. J. Zeng, Black phosphorus: an efficient co-catalyst for charge separation and enhanced photocatalytic hydrogen evolution, *J. Mater. Sci.*, 2018, **53**, 16557–16566, DOI: **10.1007/s10853-018-2830-2**.

7 Y. H. Huang, L. J. Yan, B. Wang, B. Shao, Y. Y. Niu, X. P. Zhang, P. Yin, Y. Q. Ge, W. Sun and H. Zhang, Recent applications of black phosphorus and its related composites in electrochemistry and bioelectrochemistry: a mini review, *Electrochem. Commun.*, 2021, **129**, 107095, DOI: **10.1016/j.elecom.2021.107095**.

8 S. W. Lee, F. Yang, J. K. Suh, S. J. Yang, Y. B. Lee, G. Li, H. S. Choe, A. H. Suslu, Y. B. Chen, C. Y. Ko, J. S. Park, K. Liu, J. B. Li, K. Hippalgaonkar, J. J. Urban, S. Tongay and J. Q. Wu, Anisotropic in-plane thermal conductivity of black phosphorus nanoribbons at temperatures higher than 100K, *Nat. Commun.*, 2015, **6**, 8573–8579, DOI: **10.1038/ncomms9573**.

9 X. L. Niu, W. Z. Weng, C. X. Yin, Y. Y. Niu, G. J. Li, R. X. Dong, Y. L. Men and W. Sun, Black phosphorene modified glassy carbon electrode for the sensitive voltammetric detection of rutin, *J. Electroanal. Chem.*, 2018, **811**, 78–83, DOI: **10.1016/j.jelechem.2018.01.038**.

10 X. Y. Li, X. L. Niu, W. S. Zhao, W. Chen, C. X. Yin, Y. L. Men, G. J. Li and W. Sun, Black phosphorene and PEDOT: PASS-modified electrode for electrochemistry of hemoglobin, *Electrochem. Commun.*, 2018, **86**, 68–71, DOI: **10.1016/j.elecom.2017.11.017**.

11 Y. Zhao, Y. H. Zhang, Z. Zhuge, Y. H. Tang, J. W. Tao and Y. Chen, Synthesis of a poly-L-lysine/black phosphorus hybrid for biosensors, *Anal. Chem.*, 2018, **90**, 3149–3155, DOI: **10.1021/acs.analchem.7b04395**.

12 F. Shi, B. L. Wang, L. J. Yan, Y. Y. Niu, L. S. Wang and W. Sun, *In situ* growth of nitrogen-doped carbonized polymer dots on black phosphorus for electrochemical DNA biosensor of *Escherichia coli* O157: H7, *Bioelectrochemistry*, 2022, **148**, 108226, DOI: **10.1016/j.bioelechem.2022.108226**.

13 Y. Xiang, M. B. Camarada, Y. P. Wen, H. Wu, J. Y. Chen, M. F. Li and X. N. Liao, Simple voltametric analyses of ochratoxin A in food samples using highly-stable and anti-fouling black phosphorene nanosensor, *Electrochim. Acta*, 2018, **282**, 490–498, DOI: **10.1016/j.electacta.2018.06.055**.

14 Y. Ge, M. B. Camarada, L. J. Xu, M. R. Qu, H. Liang, E. L. Zhao, M. F. Li and Y. P. Wen, A highly stable black phosphorene nanocomposite for voltametric detection of clenbuterol, *Microchim. Acta*, 2018, **185**, 566, DOI: **10.1007/s00604-018-3084-z**.

15 S. Ramalingam, R. Chand, C. B. Singh and A. Singh, Phosphorene-gold nanocomposite based microfluidic aptasensor for the detection of okadaic acid, *Biosens. Bioelectron.*, 2019, **135**, 14–21, DOI: **10.1016/j.bios.2019.03.056**.

16 Z. W. Zhao, W. Lei, X. B. Zhang, B. P. Wang and H. L. Jiang, ZnO-based amperometric enzyme biosensors, *Sensors*, 2010, **10**, 1216–1231, DOI: **10.3390/s100201216**.

17 B. X. Gu, C. X. Xu, G. P. Zhu, S. Q. Liu, L. Y. Chen, M. L. Wang and J. J. Zhu, Layer by layer immobilized horseradish peroxidase on zinc oxide nanorods for biosensing, *J. Phys. Chem. B*, 2009, **113**, 6553–6557, DOI: **10.1021/jp900048m**.

18 H. C. Ding, L. Zhang, Z. R. Tang, Y. P. Dong and X. F. Chu, Black phosphorus quantum dots doped ZnO nanoparticles as efficient electrode materials for sensitive hydrogen peroxide detection, *J. Electroanal. Chem.*, 2018, **824**, 161–168, DOI: **10.1016/j.jelechem.2018.07.055**.

19 S. T. Li, P. F. Wang, R. D. Wang, Y. F. Liu, R. S. Jing, Z. Li, Z. L. Meng, Y. Y. Liu and Q. Zhang, One-step co-precipitation method to construct black phosphorus nanosheets/ZnO nanohybrid for enhanced visible light photocatalytic activity, *Appl. Surf. Sci.*, 2019, **497**, 143682, DOI: **10.1016/j.apsusc.2019.143682**.

20 Q. Li, Y. Cen, J. Y. Huang, X. J. Li, H. Zhang, Y. F. Geng, B. I. Yakobson, Y. Du and X. Q. Tian, Zinc oxide-black phosphorus composites for ultrasensitive nitrogen dioxide sensing, *Nanoscale Horiz.*, 2018, **3**, 525–531, DOI: **10.1039/C8NH00052B**.

21 J. H. Kang, J. D. Wood, S. A. Wells, J. H. Lee, X. L. Liu, K. S. Chen and M. C. Hersam, Solvent exfoliation of

electronic-grade, two-dimensional black phosphorus, *ACS Nano*, 2015, **9**, 3596–3604, DOI: 10.1021/acsnano.5b01143.

22 P. Yasaei, B. Kumar, T. Foroozan, C. H. Wang, M. Asadi, D. Tuschel, J. E. Indacochea, R. F. Klie and A. Salehi-Khojin, High-quality black phosphorus atomic layers by liquid-phase exfoliation, *Adv. Mater.*, 2015, **27**, 1887–1892, DOI: 10.1002/adma.201405150.

23 L. J. Wang, Y. F. Qi, H. Li, R. Q. Guan, F. L. Zhang, Q. F. Zhou, D. D. Wu, Z. Zhao, G. Zhou and Z. C. Sun, Au/g-C_3N_4 heterostructure sensitized by black phosphorus for full solar spectrum waste-to-hydrogen conversion, *Sci. China Mater.*, 2022, **65**, 974–984, DOI: 10.1007/s40843-021-1833-1.

24 W. Sun, Y. Z. Li, Y. Y. Duan and K. Jiao, Direct electrocatalytic oxidation of adenine and guanine on carbon ionic liquid electrode and the simultaneous determination, *Biosens. Bioelectron.*, 2008, **24**, 988–993, DOI: 10.1016/j.bios.2008.07.068.

25 S. Wang, B. C. Zhu, M. J. Liu, L. Y. Zhang, J. G. Yu and M. H. Zhou, Direct Z-scheme ZnO/CdS hierarchical photocatalyst for enhanced photocatalytic H_2-production activity, *Appl. Catal., B*, 2019, **243**, 19–26, DOI: 10.1016/j.apcatb.2018.10.019.

26 K. Kotsis and V. Staemmler, *Ab initio* calculations of the O1s XPS spectra of ZnO and Zn oxo compounds, *Phys. Chem. Chem. Phys.*, 2006, **8**, 1490–1498, DOI: 10.1039/B515699H.

27 M. Zhu, C. Zhai, M. Fujitsuka and T. Majima, Noble metal-free near-infrared-driven photocatalyst for hydrogen production based on 2D hybrid of black phosphorus/WS_2, *Appl. Catal., B*, 2018, **221**, 645–651, DOI: 10.1016/j.apcatb.2017.09.063.

28 M. Akbari and S. Sharifnia, Synthesis of ZnS/ZnO nanocomposite through solution combustion method for high rate photocatalytic conversion of CO_2 and CH_4, *Mater. Lett.*, 2017, **194**, 110–113, DOI: 10.1016/j.matlet.2017.02.020.

29 Y. Al-Hadeethi, A. Umar, S. H. Al-Heniti, R. Kumar, S. H. Kim, X. Zhang and B. M. Raffah, 2D Sn-doped ZnO ultrathin nanosheet networks for enhanced acetone gas sensing application, *Ceram. Int.*, 2017, **43**, 2418–2423, DOI: 10.1016/j.ceramint.2016.11.031.

30 G. Abellán, C. Neiss, V. Lloret, S. Wild, J. C. Chacón-Torres, K. Werbach, F. Fedi, H. Shiozawa, A. Görling, H. Peterlik, T. Pichler, F. Hauke and A. Hirsch, Exploring the formation of black phosphorus intercalation compounds with alkali metals, *Angew. Chem., Int. Ed.*, 2017, **56**, 15267–15273, DOI: 10.1002/anie.201707462.

31 Y. Huang, Z. T. Han, X. Zhou, J. X. Li, X. L. Gu, Z. F. Li, W. Sun and X. L. Niu, Three-dimensional MoS_2-graphene aerogel nanocomposites for electrochemical sensing of quercetin, *Microchim. Acta*, 2022, **189**, 299, DOI: 10.1007/s00604-022-05336-z.

32 X. L. Cui, D. L. Jiang, P. Diao, J. X. Li, R. T. Tong and X. K. Wang, Assessing the apparent effective thickness of alkanethiol self-assembled monolayers in different concentrations of Fe $(CN)_6^{3-}$/Fe $(CN)_6^{4-}$ by acimpedance spectroscopy, *J. Electroanal. Chem.*, 1999, **470**, 9–13, DOI: 10.1016/S0022-0728(99)00201-6.

33 A. Keziban, $CuFe_2O_4$/reduced graphene oxide nanocomposite decorated with gold nanoparticles as a new electrochemical sensor material for L-cysteine detection, *J. Alloys Compd.*, 2019, **791**, 391–401, DOI: 10.1016/j.jallcom.2019.03.303.

34 J. D. Ayad, A. Keziban, Z. B. Salih and O. Mustafa, Ag-TiO_2-reduced graphene oxide hybrid film for electrochemical detection of 8-hydroxy-2′-deoxyguanosine as an oxidative DNA damage biomarker, *Anal. Methods*, 2020, **12**, 499–506, DOI: 10.1039/C9AY02175B.

35 Y. Y. Niu, R. Y. Zou, H. A. Yones, X. B. Li, X. Y. Li, X. L. Niu, Y. Chen, P. Li and W. Sun, Electrochemical behavior of horseradish peroxidase on WS_2 nanosheet-modified electrode and electrocatalytic investigation, *J. Chin. Chem. Soc.*, 2018, **65**, 1127–1135, DOI: 10.1002/jccs.201800054.

36 X. J. Liu, T. Chen, L. F. Liu and G. X. Li, Electrochemical characteristics of heme proteins in hydroxyethylcellulose film, *Sens. Actuators, B*, 2006, **113**, 106–111, DOI: 10.1016/j.snb.2005.02.029.

37 E. Laviron, The use of linear potential sweep voltammetry and of a.c. voltammetry for the study of the surface electrochemical reaction of strongly adsorbed systems and of redox modified electrodes, *J. Electroanal. Chem.*, 1979, **100**, 263–270, DOI: 10.1016/S0022-0728(79)80167-9.

38 E. Laviron, General expression of the linear potential sweep voltammogram in the case of diffusionless electrochemical systems, *J. Electroanal. Chem.*, 1979, **101**, 19–28, DOI: 10.1016/S0022-0728(79)80075-3.

39 T. R. Zhan, X. J. Wang, Y. M. Zhang, Y. Song, X. L. Liu, J. Xu and W. G. Hou, Direct electrochemistry and electrocatalysis of hemoglobin immobilized in layered double hydroxides modified with amino functionalized ionic liquid through coprecipitation technique, *Sens. Actuators, B*, 2015, **220**, 1232–1240, DOI: 10.1016/j.snb.2015.07.043.

40 X. M. Feng, R. M. Li, C. H. Hu and W. H. Hou, Direct electron transfer and electrocatalysis of hemoglobin immobilized on graphene-Pt nanocomposite, *J. Electroanal. Chem.*, 2011, **657**, 28–33, DOI: 10.1016/j.jelechem.2011.03.004.

41 F. Shi, W. Zheng, W. Wang, F. Hou, B. Lei, Z. Sun and W. Sun, Application of graphene-copper sulfide nanocomposite modified electrode for electrochemistry and electrocatalysis of hemoglobin, *Biosens. Bioelectron.*, 2015, **64**, 131–137, DOI: 10.1016/j.bios.2014.08.064.

42 W. Sun, Y. Q. Guo, T. T. Li, X. M. Ju, J. Lou and C. X. Ruan, Electrochemistry of horseradish peroxidase entrapped in graphene and dsDNA composite modified carbon ionic liquid electrode, *Electrochim. Acta*, 2012, **75**, 381–386, DOI: 10.1016/j.electacta.2012.05.018.

43 R. S. Nicholson and I. Shain, Theory of stationary electrode polarography for a chemical reaction coupled between two charge transfers, *Anal. Chem.*, 1965, **37**, 178–190, DOI: 10.1021/2Fac60221a002.

44 S. F. Wang, F. Xie and G. D. Liu, Direct electrochemistry and electrocatalysis of heme proteins on SWCNTs-CTAB modified electrodes, *Talanta*, 2009, **77**, 1343–1350, DOI: 10.1016/j.talanta.2008.09.019.

45 X. J. Han, W. M. Huang, J. B. Jia, S. J. Dong and E. K. Wang, Direct electrochemistry of hemoglobin in egg-phosphatidylcholine films and its catalysis to H_2O_2, *Biosens. Bioelectron.*, 2002, **17**, 741–746, DOI: 10.1016/S0956-5663(02)00052-0.

46 T. R. Zhan, Z. W. Tan, X. J. Wang and W. G. Hou, Hemoglobin immobilized in g-C_3N_4 nanoparticle decorated 3D graphene-LDH network: direct electrochemistry and electrocatalysis to trichloroacetic acid, *Sens. Actuators, B*, 2018, **255**, 149–158, DOI: 10.1016/j.snb.2017.08.048.

47 W. Ma and D. Tian, Direct electron transfer and electrocatalysis of hemoglobin in ZnO coated multiwalled carbon nanotubes and Nafion composite matrix, *Bioelectrochemistry*, 2010, **78**, 106–112, DOI: 10.1016/j.bioelechem.2009.08.002.

48 Y. Z. Liu, R. Mao, Y. T. Tong, H. C. Lan, G. Zhang, H. J. Liu and J. H. Qu, Reductive dechlorination of trichloroacetic acid (TCAA) by electrochemical process over Pd-In/Al_2O_3 catalyst, *Electrochim. Acta*, 2017, **232**, 13–21, DOI: 10.1016/j.electacta.2017.02.071.

49 T. R. Zhan, X. J. Wang, X. J. Li and W. G. Hou, Hemoglobin immobilized in exfoliated Co_2AlLDH-graphene nanocomposite film: direct electrochemistry and electrocatalysis toward trichloroacetic acid, *Sens. Actuators, B*, 2016, **228**, 101–108, DOI: 10.1016/j.snb.2015.12.095.

50 E. Wierzbicka, Novel methods of nitrate and nitrite determination: a review, *J. Elem.*, 2020, **25**, 97–106, DOI: 10.5601/jelem.2019.24.3.1848.

51 Y. Ding, Y. Wang and Y. Lei, Direct electrochemistry and electrocatalysis of novel single-walled carbon nanotubes-hemoglobin composite micro belts-towards the development of sensitive and mediator-free biosensor, *Biosens. Bioelectron.*, 2010, **26**, 390–397, DOI: 10.1016/j.bios.2010.07.124.

52 A. E. F. Nassar, J. M. Bobbitt, J. D. Stuart and J. F. Rusling, Catalytic reduction of organohalide pollutants by myoglobin in a biomembrane-like surfactant film, *J. Am. Chem. Soc.*, 1995, **117**, 10986–10993, DOI: 10.1021/ja00149a022.

53 K. A. Johnson and R. S. Goody, The original michaelis constant: translation of the 1913 michaelis-menten paper, *Biochemistry*, 2011, **50**, 8264–8269, DOI: 10.1021/bi201284u.

54 J. Liu, W. J. Weng, H. Xie, G. L. Luo, G. J. Li, W. Sun, C. X. Ruan and X. H. Wang, Myoglobin and hydroxyapatite-doped carbon nanofiber-modified electrodes for electrochemistry and electrocatalysis, *ACS Omega*, 2019, **4**, 15653–15659, DOI: 10.1021/acsomega.9b02151.

55 Z. H. Zhu, X. Li, Y. Wang, Y. Zeng, W. Sun and X. T. Huang, Direct electrochemistry and electrocatalysis of horseradish peroxidase with hyaluronic acid-ionic liquid-cadmium sulfide nanorod composite material, *Anal. Chim. Acta*, 2010, **670**, 51–56, DOI: 10.1016/j.aca.2010.04.061.

56 F. Shi, W. Wang, S. Gong, B. Lei, G. Li, X. Lin, Z. Sun and W. Sun, Application of titanium dioxide nanowires for the direct electrochemistry of hemoglobin and electrocatalysis, *J. Chin. Chem. Soc.*, 2015, **62**, 554–561, DOI: 10.1002/jccs.201400373.

57 Y. Y. Niu, X. Y. Li, H. Xie, G. L. Luo, R. Y. Zou, Y. R. Xi, G. J. Li and W. Sun, Electrochemical performance and electrocatalytic behavior of myoglobin on graphene tube-modified electrode, *J. Chin. Chem. Soc.*, 2020, **67**, 1054–1061, DOI: 10.1002/jccs.201900282.

58 W. Chen, W. J. Weng, X. L. Niu, X. Y. Li, Y. L. Men, W. Sun, G. J. Li and L. F. Dong, Boron-doped graphene quantum dots modified electrode for electrochemistry and electrocatalysis of hemoglobin, *J. Electroanal. Chem.*, 2018, **823**, 137–145, DOI: 10.1016/j.jelechem.2018.06.001.

59 G. Y. Chen, H. Sun and S. F. Hou, Electrochemistry and electrocatalysis of myoglobin immobilized in sulfonated graphene oxide and Nafion films, *Anal. Biochem.*, 2016, **502**, 43–49, DOI: 10.1016/j.ab.2016.03.003.

60 H. Xie, G. L. Luo, Y. Y. Niu, W. J. Weng, Y. X. Zhao, Z. Q. Li, C. X. Ruan, G. J. Li and W. Sun, Synthesis and utilization of Co_3O_4 doped carbon nanofiber for fabrication of hemoglobin-based electrochemical sensor, *Mater. Sci. Eng., C*, 2020, **107**, 110209, DOI: 10.1016/j.msec.2019.110209.

61 G. L. Turdean and G. Szabo, Nitrite detection in meat products samples by square-wave voltammetry at a new single walled carbon naonotubes-myoglobin modified electrode, *Food Chem.*, 2015, **179**, 325–330, DOI: 10.1016/j.foodchem.2015.01.106.

62 X. Y. Li, G. L. Luo, H. Xie, Y. Y. Niu, X. B. Li, R. Y. Zou, Y. R. Xi, Y. Xiong, W. Sun and G. J. Li, Voltammetric sensing performances of a carbon ionic liquid electrode modified with black phosphorene and hemin, *Microchim. Acta*, 2019, **186**, 304–312, DOI: 10.1007/s00604-019-3421-x.